

Microglial activation and tau burden predict cognitive decline in Alzheimer's disease

 Maura Malpetti,¹  Rogier A. Kievit,²  Luca Passamonti,^{1,3}  P. Simon Jones,¹
 Kamen A. Tsvetanov,¹  Timothy Rittman,¹  Elijah Mak,⁴  Nicolas Nicastro,^{4,5}
W. Richard Bevan-Jones,⁴ Li Su,⁴ Young T. Hong,¹ Tim D. Fryer,¹ Franklin I. Aigbirhio,¹
John T. O'Brien^{4,6,*} and  James B. Rowe^{1,2,6,*}

*These authors contributed equally to this work.

Tau pathology, neuroinflammation, and neurodegeneration are key aspects of Alzheimer's disease. Understanding whether these features predict cognitive decline, alone or in combination, is crucial to develop new prognostic measures and enhanced stratification for clinical trials. Here, we studied how baseline assessments of *in vivo* tau pathology (measured by ¹⁸F-AV-1451 PET), neuroinflammation (measured by ¹¹C-PK11195 PET) and brain atrophy (derived from structural MRI) predicted longitudinal cognitive changes in patients with Alzheimer's disease pathology. Twenty-six patients ($n = 12$ with clinically probable Alzheimer's dementia and $n = 14$ with amyloid-positive mild cognitive impairment) and 29 healthy control subjects underwent baseline assessment with ¹⁸F-AV-1451 PET, ¹¹C-PK11195 PET, and structural MRI. Cognition was examined annually over the subsequent 3 years using the revised Addenbrooke's Cognitive Examination. Regional grey matter volumes, and regional binding of ¹⁸F-AV-1451 and ¹¹C-PK11195 were derived from 15 temporo-parietal regions characteristically affected by Alzheimer's disease pathology. A principal component analysis was used on each imaging modality separately, to identify the main spatial distributions of pathology. A latent growth curve model was applied across the whole sample on longitudinal cognitive scores to estimate the rate of annual decline in each participant. We regressed the individuals' estimated rate of cognitive decline on the neuroimaging components and examined univariable predictive models with single-modality predictors, and a multi-modality predictive model, to identify the independent and combined prognostic value of the different neuroimaging markers. Principal component analysis identified a single component for the grey matter atrophy, while two components were found for each PET ligand: one weighted to the anterior temporal lobe, and another weighted to posterior temporo-parietal regions. Across the whole-sample, the single-modality models indicated significant correlations between the rate of cognitive decline and the first component of each imaging modality. In patients, both stepwise backward elimination and Bayesian model selection revealed an optimal predictive model that included both components of ¹⁸F-AV-1451 and the first (i.e. anterior temporal) component for ¹¹C-PK11195. However, the MRI-derived atrophy component and demographic variables were excluded from the optimal predictive model of cognitive decline. We conclude that temporo-parietal tau pathology and anterior temporal neuroinflammation predict cognitive decline in patients with symptomatic Alzheimer's disease pathology. This indicates the added value of PET biomarkers in predicting cognitive decline in Alzheimer's disease, over and above MRI measures of brain atrophy and demographic data. Our findings also support the strategy for targeting tau and neuroinflammation in disease-modifying therapy against Alzheimer's disease.

- 1 Department of Clinical Neurosciences, University of Cambridge, Cambridge, UK
- 2 MRC Cognition and Brain Sciences Unit, University of Cambridge, Cambridge, UK
- 3 Institute of Molecular Bioimaging and Physiology, National Research Council, Milano, Italy
- 4 Department of Psychiatry, University of Cambridge, Cambridge, UK
- 5 Department of Clinical Neurosciences, Geneva University Hospitals, Switzerland
- 6 Cambridge University Hospitals NHS Trust, Cambridge, UK

Received October 28, 2019. Revised January 9, 2020. Accepted February 7, 2020

© The Author(s) (2020). Published by Oxford University Press on behalf of the Guarantors of Brain.

This is an Open Access article distributed under the terms of the Creative Commons Attribution License (<http://creativecommons.org/licenses/by/4.0/>), which permits unrestricted reuse, distribution, and reproduction in any medium, provided the original work is properly cited.

Correspondence to: Prof. James B. Rowe
 Department of Clinical Neurosciences
 University of Cambridge
 Herchel Smith Building, Forvie Site
 Robinson Way, Cambridge Biomedical Campus
 Cambridge, CB2 0SZ, UK
 E-mail: james.rowe@mrc-cbu.cam.ac.uk

Keywords: Alzheimer's disease; neuroinflammation; tau pathology; PET imaging; cognitive decline

Abbreviations: ACE-R = revised Addenbrooke's Cognitive Examination; BP_{ND} = non-displaceable binding potential; CFI = comparative fit index; LGCM = latent growth curve model; MCI = mild cognitive impairment; RMSEA = root-mean-square error of approximation; SRMR = standardized root mean-square residual

Introduction

The pathological hallmarks of Alzheimer's disease are tau neurofibrillary tangles and amyloid- β plaques, but neuroinflammation has also emerged as a key process in Alzheimer's disease and other neurodegenerative disorders (Pasqualetti et al., 2015; Ransohoff, 2016; Schain and Kreisl, 2017). The differential role of these pathologies in predicting clinical progression of Alzheimer's disease remains to be ascertained. This represents a critical step to develop new prognostic markers and test the effect of novel disease-modifying therapies that target different pathologies in Alzheimer's disease.

The aggregation of misfolded tau protein is associated with synaptic dysfunction and neuronal loss, and correlates with clinical severity in the Alzheimer's disease clinical spectrum (Nelson et al., 2012; Spires-Jones and Hyman, 2014). A significant presence of amyloid- β plaques is also indicative of likely cognitive decline in mid- and later-life, although the association of both neurodegeneration and cognitive impairment has been found stronger with the distribution and burden of neurofibrillary tangles than it is for neuritic plaques (Nelson et al., 2012; Spires-Jones and Hyman, 2014). Microglia activation and neuroinflammation represent a third key determinant in the aetiopathogenesis of Alzheimer's disease and in its progression (Heneka et al., 2015; Mhatre et al., 2015; Calsolaro and Edison, 2016), independently or synergistically with tau and amyloid pathology.

Each of these processes can now be quantified and localized *in vivo* using brain imaging, such as PET imaging with radioligands targeting tau pathology, amyloid burden, and microglial activation (see Chandra et al., 2019 for a review). The PET ligand ^{18}F -AV-1451 is sensitive to cortical tau accumulation in Alzheimer's disease, and has high affinity for the characteristic paired helical tau filaments (Xia et al., 2013; Marquie et al., 2015; Lowe et al., 2016). ^{18}F -AV-1451 PET studies have shown marked tau accumulation in the entorhinal cortex in patients with mild cognitive impairment (MCI) that extends to temporo-parietal regions in Alzheimer's disease (Hall et al., 2017). ^{18}F -AV-1451

bindings also correlates with Braak staging of neurofibrillary tau (Schöll et al., 2016; Schwarz et al., 2016), and post-mortem patterns of Alzheimer's disease pathology (Sander et al., 2016; Lowe et al., 2020; Smith et al., 2019). This is also in keeping with evidence that tau deposition is evident as a continuum from normal ageing through MCI to Alzheimer's dementia (Schöll et al., 2019), and correlates with cognitive impairment (Brier et al., 2016; Cho et al., 2016b; Johnson et al., 2016; Ossenkoppele et al., 2016; Pontecorvo et al., 2017). In addition, PET imaging supported the previous evidence of a stronger association of cognitive deficits with tau burden than with amyloid- β (Brier et al., 2016; Johnson et al., 2016).

The PET ligand ^{11}C -PK11195 is a well-established marker for microglial activation via its binding to the 18-kDa translocator protein (TSPO), a mitochondrial membrane protein that is overexpressed in activated microglia (Scarf and Kassiou, 2011). Results with this ligand in Alzheimer's disease have been variable (for a review see Chandra et al., 2019), but this may be due to small sample sizes and inconsistent methods between previous *in vivo* studies. ^{11}C -PK11195 has shown high binding in temporo-parietal regions and cingulate cortex in patients with Alzheimer's disease (Stefaniak and O'Brien, 2015), while neuroinflammation in these regions is inversely associated with cognitive performance in MCI and Alzheimer's dementia (Edison et al., 2008; Okello et al., 2009a; Fan et al., 2015a; Passamonti et al., 2018, 2019). However, inflammation does not correlate well with amyloid burden (Yokokura et al., 2011), suggesting an independent role of microglia activation in leading to cognitive deficits.

There are extensive data on atrophy in Alzheimer's disease, measured in terms of volume loss *in vivo* by MRI, at MCI and dementia stages of progressive Alzheimer's disease pathology. For example, MRI measures of medial temporal lobe volumes correlate with disease severity, and are predictive of future conversion from MCI to Alzheimer's disease (Frisoni et al., 2010; Leung et al., 2013; Jack et al., 2015). However, cell loss and atrophy are relatively late features in a cascade of pathology, and it is not clear how MRI compares with measures of molecular pathology as a prognostic

marker, especially in view of marked age-related structural changes (Raz *et al.*, 2005; Walhovd *et al.*, 2011).

In this study, we test the ability of baseline *in vivo* measures of tau pathology, microglia activation, and brain atrophy to predict the rate of cognitive decline in patients with Alzheimer's disease pathology, ranging from MCI (with biomarker evidence of amyloid pathology) to clinically probable Alzheimer's disease (with dementia). Our hypothesis was that the PET biomarkers of tau pathology and neuroinflammation are strong predictors of cognitive impairment and decline, and that whereas MRI may be predictive in isolation, the prognostic information of MRI is better captured by direct PET measures of molecular pathology (Bejanin *et al.*, 2017; Mattsson *et al.*, 2019). This hypothesis builds on evidence that tau burden relates to age-related cognitive decline (Schöll *et al.*, 2016; Aschenbrenner *et al.*, 2018; Maass *et al.*, 2018), and progression of dementia over 6 to 18 months in patients with Alzheimer's disease (Koychev *et al.*, 2017; Pontecorvo *et al.*, 2019). In contrast to past studies that assessed the relationship between longitudinal PET markers and clinical changes in Alzheimer's disease (Fan *et al.*, 2015b, 2017, Chiotis *et al.*, 2018; Jack *et al.*, 2018; Southekal *et al.*, 2018; Cho *et al.*, 2019), we studied how a multi-modal and cross-sectional assessment of distinct pathologies is able to predict longitudinal decline in Alzheimer's disease, examining the individual or combined prognostic contribution of tau pathology, neuroinflammation, and brain atrophy in predicting cognitive decline.

The better characterization of the factors predicting decline in Alzheimer's disease will help to develop enhanced prognostic and outcome measures for clinical trials targeting more than one pathology. Although previous findings support the use of MRI and PET imaging in the diagnosis and monitoring of disease progression, the prognostic value of these *in vivo* measures and their combined effect in predicting clinical decline in Alzheimer's disease remains undetermined. Previous studies that have evaluated the predictive values of neuroimaging markers in Alzheimer's disease have typically assessed different neuroimaging modalities in isolation rather than exploiting the mechanistic and prognostic values that are offered by multi-modal neuroimaging. We therefore assessed the independent and combined predictive effects of baseline neuroimaging biomarkers for tau pathology (^{18}F -AV-1451 PET), neuroinflammation (^{11}C -PK11195 PET) and brain atrophy (structural MRI) on longitudinal cognitive changes over a period of 3 years in the clinical spectrum of Alzheimer's disease. Given the published evidence of dominant involvement of temporal and parietal brain regions in early neurodegeneration, tau pathology, and neuroinflammation in Alzheimer's disease (Garibotto *et al.*, 2017; Jagust, 2018; Whitwell, 2018), we decided *a priori* to focus our analyses on these regions. Pathology may occur in frontal and occipital regions, but for typical amnesic phenotypes, we considered this to be of secondary importance. In the temporo-parietal regions there is a hierarchical evolution in tau pathology and atrophy from MCI to Alzheimer's

dementia, recapitulating neuropathological staging and correlating with clinical severity (for a review see Jagust, 2018).

We predicted: (i) a significant association between baseline measures of each neuroimaging technique and longitudinal decline in cognition; (ii) partially independent and additive effects of MRI and PET measures on cognitive decline, assessed with all modalities together in a single multivariate model; and (iii) that the molecular markers of baseline tau and neuroinflammation PET would be more informative than structural MRI on longitudinal cognitive deterioration in Alzheimer's disease.

Material and methods

Participants

We recruited 26 patients: 12 with a clinical diagnosis of probable Alzheimer's dementia and 14 with amnesic MCI and a positive amyloid PET scan as biomarker of Alzheimer's disease (Klunk *et al.*, 2004). Probable Alzheimer's dementia was diagnosed according to the National Institute on Aging-Alzheimer's Association guidelines (McKhann *et al.*, 2011) and confirmed in all patients during follow-up. Given the long-term and intensive nature of the longitudinal project, all patients at baseline had >12/30 on the Mini-Mental State Examination (MMSE) to be eligible to participate in the study. MCI patients had MMSE score >24/30, and memory impairment not ascribable another diagnosis (Albert *et al.*, 2011). We also included 29 healthy controls with MMSE >26/30, absence of memory symptoms, no signs of dementia, or any other significant medical illnesses.

All gave informed consent according to the Declaration of Helsinki. The NIMROD protocol [Neuroimaging of Inflammation in Memory and Related Other Disorders (Bevan-Jones *et al.*, 2017)] was approved by the NIHR National Research Ethic Service Committee and East of England (Cambridge Central).

During the first visit, demographic information and medical history were collected. All participants underwent a baseline neuropsychological assessment, followed by an MRI scan and one, two or three PET scans depending on the group. The clinical examination and neuropsychological battery were repeated annually for three follow-up visits (for details see Bevan-Jones *et al.*, 2017). The revised Addenbrooke's Cognitive Examination (ACE-R) (Mioshi *et al.*, 2006) was used to assess the cognitive performance at each visit. All patients diagnosed with Alzheimer's dementia deteriorated significantly in the follow-up clinical visits compared to the study baseline. Six of 14 patients with MCI were clinically diagnosed as converting to Alzheimer's disease and/or presented MMSE \leq 24/30 by the end of the study (3 years), and three further patients subsequently.

Imaging data acquisition and preprocessing

All subjects underwent 3 T MRI performed on a Siemens Magnetom Tim Trio or Verio scanner (Siemens). A T₁-weighted MPRAGE image was acquired for each participant (repetition time = 2300 ms, echo time = 2.98 ms, field of view = 240 × 256 mm², 176 slices of 1-mm thickness, flip angle = 9°).

MCI and Alzheimer's dementia subjects had both dynamic ¹⁸F-AV-1451 PET and ¹¹C-PK11195 PET, while, to minimize radiation exposure in healthy individuals, control subjects were divided into two groups: 14 underwent ¹⁸F-AV-1451 PET, while another 15 underwent ¹¹C-PK11195 PET. PET scanning was undertaken on a GE Advance PET scanner (GE Healthcare) and a GE Discovery 690 PET/CT (Supplementary Table 1). Patients with MCI also underwent 40–70 min post-injection ¹¹C-PiB PET to quantify the density of fibrillar amyloid-β deposits for classification of amyloid-β status. The emission protocols were: 90 min dynamic imaging following a 370 MBq ¹⁸F-AV-1451 injection; 75 min of dynamic imaging starting concurrently with a 500 MBq ¹¹C-PK11195 injection; and 550 MBq ¹¹C-PiB injection followed by imaging from 40–70 min post-injection (for details see Passamonti et al., 2017, 2018). All images were reconstructed with PROMIS 3D filtered back-projection (Kinahan and Rogers, 1989), with the Colsher filter apodized with a transaxial Hann filter cut-off at the Nyquist frequency. Corrections for dead time, randoms, normalization, scatter, attenuation, and sensitivity were included in the image reconstruction process. ¹¹C-PiB scans were classified as positive if the average standardized uptake value ratio (SUVR) across the cortex using a cerebellar grey matter reference region was > 1.5 (Villemagne et al., 2013). This threshold was chosen to minimize false positives (Jack et al., 2008; Villemagne et al., 2011). Only MCI patients with positive amyloid-β status were included in this study, and were combined with patients with Alzheimer's dementia as these two groups are thought to represent a continuum of the same clinical and pathological spectrum (Okello et al., 2009b).

Structural imaging data were processed in SPM12. The T₁-weighted images were segmented into grey matter, white matter and CSF and used to determine regional grey matter, white matter and CSF volumes, and to calculate brain volume (grey + white matter) and total intracranial volume (TIV = grey matter + white matter + CSF) in each participant. The grey and white matter segments from 33 subjects were used to create an unbiased template (11 controls, 11 patients with MCI and 11 patients with Alzheimer's dementia, matched for age and sex across the groups) using the DARTEL pipeline in SPM12. The images from the remaining 22 participants were warped to the template to bring all participants into the same space. Segmented images were then warped to MNI space. The images were matched to the Hammers atlas [(Hammers et al., 2003; Gousias et al., 2008) modified to include brainstem parcellation and

the cerebellar dentate nucleus in MNI152 2009c space] to perform a region of interest analysis. The atlas comprised 83 cortical regions. The group template was warped to the ICBM MNI152 2009c template using the 'Population to ICBM' function, applied to the Hammers atlas in DARTEL template space, followed by linear transformation to MNI space. These steps place the regions of interest in the same space as the individual normalized MRI images. Individual regional grey matter volumes were then extracted using the 'spm_summarise' function.

For each subject, the aligned PET image series for each scan was rigidly co-registered to the T₁-weighted MRI image. Prior to kinetic modelling, regional PET data were corrected for CSF contamination by dividing by the mean region grey plus white matter fraction determined from SPM tissue probability maps smoothed to PET spatial resolution. For ¹¹C-PK11195, supervised cluster analysis was used to determine the reference tissue time-activity curve and non-displaceable binding potential (BP_{ND}) was calculated in each region of interest using a simplified reference tissue model that includes correction for vascular binding (Yaquib et al., 2012). For ¹⁸F-AV-1451, BP_{ND} was assessed in each region of interest with the simplified reference tissue model (Gunn et al., 1997) using superior cerebellar cortex grey matter as the reference region. For more details about the data preprocessing steps, see Passamonti et al. (2017, 2018).

The number of regions was reduced from 83 to 15 *a priori* regions of interest by (i) combining left and right regional values in bilateral regions (*cf.* Passamonti et al., 2017, 2018); and (ii) focusing on 15 bilateral temporo-parietal regions, related to Alzheimer's disease pathology (Supplementary Table 2). Regional grey matter volumes were corrected for total intracranial volume. For both ¹¹C-PK11195 and ¹⁸F-AV-1451, a volume-weighted mean of left and right regional BP_{ND} values was calculated for each bilateral region of interest.

Statistical analyses

Descriptive statistics

Continuous variables (age, education, ACE-R) were compared between groups with an independent-samples *t*-test, and categorical variables (sex) with the chi-square test. The effect size of each *t*-test comparison was computed to quantify differences between the two groups (Cohen's *d* > 0.8, valuable difference).

Principal components analysis

The standardized values determined for the 15 bilateral regions of interest from each imaging dataset were included in three principal component analyses (PCAs), run separately for grey matter volumes, ¹¹C-PK11195 and ¹⁸F-AV-1451 BP_{ND} values. This reduces dimensionality and the problem of multiple comparisons, identifying a limited number of components that best explain the data variance. We applied an orthogonal varimax rotation to maximize interpretability and specificity of the resulting components. We retained

components with eigenvalues >1 . To test whether correction for CSF affected the PCA results, we applied the same analyses on ^{18}F -AV-1451 PET and ^{11}C -PK11195 regional data not corrected for CSF partial volume.

The individual component scores were corrected for the time interval in months between the baseline cognitive assessment and each scan. Median (mean and standard deviation, SD) of the time interval between the baseline cognitive assessment and the imaging scans were: 1.0 (1.75 ± 2.50) months for MRI, 7.5 (7.18 ± 5.68) months for ^{18}F -AV-1451 PET and 2 (6.12 ± 9.07) months for ^{11}C -PK11195 PET. The residuals extracted for each component were included in a multiple regression on cognitive decline as independent variables.

LGCM for cognitive data

ACE-R scores at follow-up were annualized to the nearest whole year, using the absolute difference in scores between the baseline and the following visits, divided by the time interval in days between tests and multiplied by 365 (1 year), 730 (2 years) or 1095 (3 years). A latent growth curve model (LGCM) was fitted on longitudinal annualized ACE-R scores across all subjects ($n = 55$), to obtain (i) the intercept; (ii) the slope, quantifying the rate of change and its form (i.e. linear or non-linear); and (iii) the relation between intercept and slope. A linear slope for the longitudinal ACE-R scores was estimated, and used in further analyses. Addition of a non-linear (quadratic) term to the model did not improve the estimation of slope ([Supplementary material](#)). The estimated parameters are based on the individuals' trajectory, indicating average change and individual difference. Covariates can be added to the model to assess their associations with both intercept and slope. Three time points and 5–10 cases per parameter are required for a standard LGCM ([Bentler and Chou, 1987](#); [Newsom, 2015](#)). LGCM was implemented in Lavaan software ([Rosseel, 2012](#)) using full information maximum likelihood estimation with robust standard errors for missingness and non-normality. We considered four indices of good model fit ([Schermelleh-Engel et al., 2003](#)): (i) the chi-square test with the P -value (good fit: >0.05); (ii) the root-mean-square error of approximation (RMSEA, acceptable fit: <0.08 , good fit: <0.05); (iii) the comparative fit index (CFI, acceptable fit: 0.95 – 0.97 , good fit: >0.97); and (iv) the standardized root mean-square residual (SRMR, acceptable fit: 0.05 – 0.10 , good fit: <0.05). From the model fitting, variables 'intercept' and 'slope' were created extracting the individual estimated values for each subject in the model. T -tests and ANOVA tested for group differences in initial cognitive performance and annual change.

One-step prediction procedure: LGCMs with predictors

Across all subjects, we tested the predictive value of each imaging method on cognitive decline, applying five LGCMs with each scan-specific component's values (corrected for months from the baseline) as predictor of cognitive intercept

and slope. Models were tested separately for MRI ($n = 55$), ^{11}C -PK11195 PET ($n = 41$) and ^{18}F -AV-1451 PET ($n = 40$). Then, in patients ($n = 26$), the individual scores of all five imaging components were included as predictors in the LGCM on longitudinal ACE-R, estimating the combined predictive effect of imaging modalities.

The one step procedure is a simple approach to our research questions, but brings estimation challenges with a modest sample size. Therefore, we next applied a two-step prediction procedure: (i) extracting individual slope values from the initial LGCM for cognitive data across all the population; and (ii) including these values as dependent variables in linear regression models with brain imaging components as predictors. We present both frequentist and Bayesian analyses to ensure inferential robustness and allowing us to quantify evidence in favour of the null hypothesis (of no predictive value).

Two-step frequentist prediction: linear regression models on LGCM parameters

First, across all subjects, the residual values of each scan-specific PCA component (corrected for months from the baseline) were included as single predictors in separated univariable linear regression models with the individual slope values extracted from the initial LGCM as dependent variable. The significance level was set at $P < 0.01$ corrected for multiple comparisons (Bonferroni correction $\alpha = 0.05/5$). Next, the individual scores of the imaging methods' components were included as independent variables in a multivariable regression analysis on patients alone ($n = 26$), who underwent all three imaging scans. This model was fit to examine the individual, as well as combined, ability to explain variance in cognitive decline using brain marker components as well as age, education, and sex as independent variables. The model used stepwise backward selection (entry criterion $\alpha = 0.05$ and elimination criterion $\alpha = 0.1$; see the [Supplementary material](#) for comparable models applied with the estimated intercept as dependent variable). A complementary *post hoc* 'exploratory' linear regression analysis included the interaction term between PET independent variables, to test whether their interaction was predictive of cognitive decline. In supplementary analyses, we applied a 'reduced' multivariable linear regression analysis with slope as dependent variable and only the first component of each imaging method as predictors to test that the different number of components between MRI and PET did not affect the estimation. These supplementary analyses were performed with and without the interaction terms between tau and inflammation measures. Given the challenges of stepwise model selection, and the limitations of sample size to utilize more advanced methods (e.g. regularized model fitting), we ran the analysis using Bayesian methodology, to ensure inferential robustness of our findings and confidence in the null results.

Two-step Bayesian prediction: linear regression models on LGCM estimated parameters

We applied a Bayesian multiple regression analysis with brain components and demographic variables as predictors, and the estimated slope values as dependent variable. This approach was used to test whether there was evidence for the absence of independent variables' effect for those components excluded from the final models (as opposed to frequentist type II error). In the model comparisons, adopting a uniform prior over the models, we considered as final model the one with the highest Bayes Factor compared to the null model (BF_{10}). Then, we used a reduced Bayesian linear regression, mirroring the reduced model applied with the frequentist approach, which included only the first component of each imaging method as predictors of slope.

One- and two-step prediction procedures

See [Supplementary Fig. 1](#) for a schematic representation of statistical analyses with one-step and two-step prediction procedures. All PCAs and regression models were performed in SPSS Statistics version 25 (IBM); all Bayesian analysis in JASP version 0.10.2 (JASP team) and all LCGMs used R version 3.6.1 (R Core Team).

Data availability

Anonymized data may be shared by request to the senior author from a qualified investigator for non-commercial use (sharing of some data is subject to restrictions according to participant consent and data protection legislation).

Results

Descriptive statistics

Significant differences between patient and control groups were found for education [$t(48.4) = 2.4, P = 0.02, d = 0.64$] and ACE-R scores [$t(33.3) = 8.6, P < 0.001, d = 2.37$]. There were no significant group differences in age [$t(53) = -1.7, P = 0.09, d = -0.47$] and sex [$\chi^2(1) = 0.17, P = 0.68$] ([Table 1](#)). Individual ACE-R scores at baseline and at each follow-up are shown in [Fig. 1](#). See [Supplementary Table 3](#) for demographics in patient and control subgroups.

Principal component analysis of grey matter volumes, $^{18}\text{F-AV-1451}$ BP_{ND} and $^{11}\text{C-PK11195}$ BP_{ND}

For grey matter volumes, the PCA on the preselected 15 Alzheimer's disease-specific cortical regions identified only one component that encompassed all the temporo-parietal regions and explained 74% of the variance ([Fig. 2](#), left). Two principal components were detected for $^{18}\text{F-AV-1451}$ BP_{ND} data, explaining 91% of the total variance (83% first

component; 8% second component). The first component was loaded onto the posterior temporal and parietal regions, while the second component was weighted to the anterior temporal lobe, amygdala, insula and hippocampus ([Fig. 2](#), middle). For $^{11}\text{C-PK11195}$ BP_{ND} data, two principal components were identified, and these explained together the 76% of data variance (56% for the first component; 20% for the second component). The first component involved anterior and medial temporal lobe, while the second component was mainly loaded onto the posterior temporo-parietal regions and insula ([Fig. 2](#), right). The loadings are shown in [Supplementary Table 4](#). Using PET data without CSF correction yielded qualitatively similar results.

Simple correlations between MRI and PET component scores across subjects were significant for the MRI component versus the first $^{11}\text{C-PK11195}$ component ($R = -0.459, P = 0.003$, significant after Bonferroni correction), but not the second $^{11}\text{C-PK11195}$ component ($R = -0.154, P = 0.337$). The MRI component was weakly associated with the first ($R = -0.319, P = 0.045$, uncorrected) and the second ($R = -0.329, P = 0.038$, uncorrected) $^{18}\text{F-AV-1451}$ components. In patients, correlations between $^{18}\text{F-AV-1451}$ and $^{11}\text{C-PK11195}$ components were not significant, even uncorrected.

Annual rate of cognitive decline

The linear LGCM of longitudinal ACE-R scores fitted the data adequately [$\chi^2(8) = 10.93, P = 0.206$; RMSEA = 0.09 (0.00–0.21), CFI = 0.99, SRMR = 0.04]. Three of four model fit indices were 'acceptable' or 'good' by [Schermelleh-Engel et al. \(2003\)](#) guidelines, although the RMSEA (>0.08) was not. To exclude a large single source of misfit, we inspected the standardized residual matrix, and confirmed no single standardized residual greater than $r = 0.099$. We therefore considered the overall model fit sufficient. The mean of the intercept was 86.40 [standard error (SE) = 1.44, z -value = 60.02, fully standardized estimate (Std Est) = 8.28, $P < 0.001$] and average cognition declined over time [slope, estimate (est) = $-3.01, SE = 0.80, z$ -value = $-3.75, Std Est = -0.54, P < 0.001$]. The intercept significantly covaried with the slope [est = 38.51, SE = 9.24, z -value = 4.17, Std Est (correlation) = 0.67, $P < 0.001$], such that individuals with higher (better) baseline performance showed less steep decline. As expected, patients significantly differed from controls in their intercept [$t(31.8) = 9.39, P < 0.001$] and slope [$t(25.9) = 6.42, P < 0.001$] indicating a faster and more severe cognitive decline ([Fig. 3](#)). Across three groups, ANOVA confirmed group differences in the intercept [$F(2) = 63.44, P < 0.001$; mean (SD) for: controls = 94.18 (3.27); MCI-positive patients = 81.25 (6.17); Alzheimer's patients = 73.60 (8.96)] and slope [$F(2) = 53.74, P < 0.001$; mean (SD) for: controls = 0.40 (0.82); MCI-positive patients = $-3.56 (3.08)$; Alzheimer's patients = $-10.62 (5.71)$], with *post hoc* confirmation of differences between each pair of groups (all $P < 0.005$).

Table 1 Demographic and clinical characteristics for the patient and control groups

	MCI +/AD patients	Healthy controls	Group difference
<i>n</i>	26	29	
Sex, female/male	12/14	15/14	$\chi^2(1) = 0.17, P = 0.68$
Age, years, mean \pm SD	72.1 \pm 8.7	68.3 \pm 7.2	$t(53) = -1.7, P = 0.09, d = -0.47$
Education, years, mean \pm SD	13.1 \pm 3.2	14.9 \pm 2.6	$t(48.4) = 2.4, P = 0.02, d = 0.64$
ACE-R Baseline, mean \pm SD	77.8 \pm 9.1	94.4 \pm 4.0	$t(33.3) = 8.6, P < 0.001, d = 2.37^*$
Disease duration, years, mean \pm SD	3.6 \pm 2.1	–	–

*Significant difference between patients and controls (P -value < 0.05) with effect size $d > 0.8$ for t -test.
AD = Alzheimer's disease.

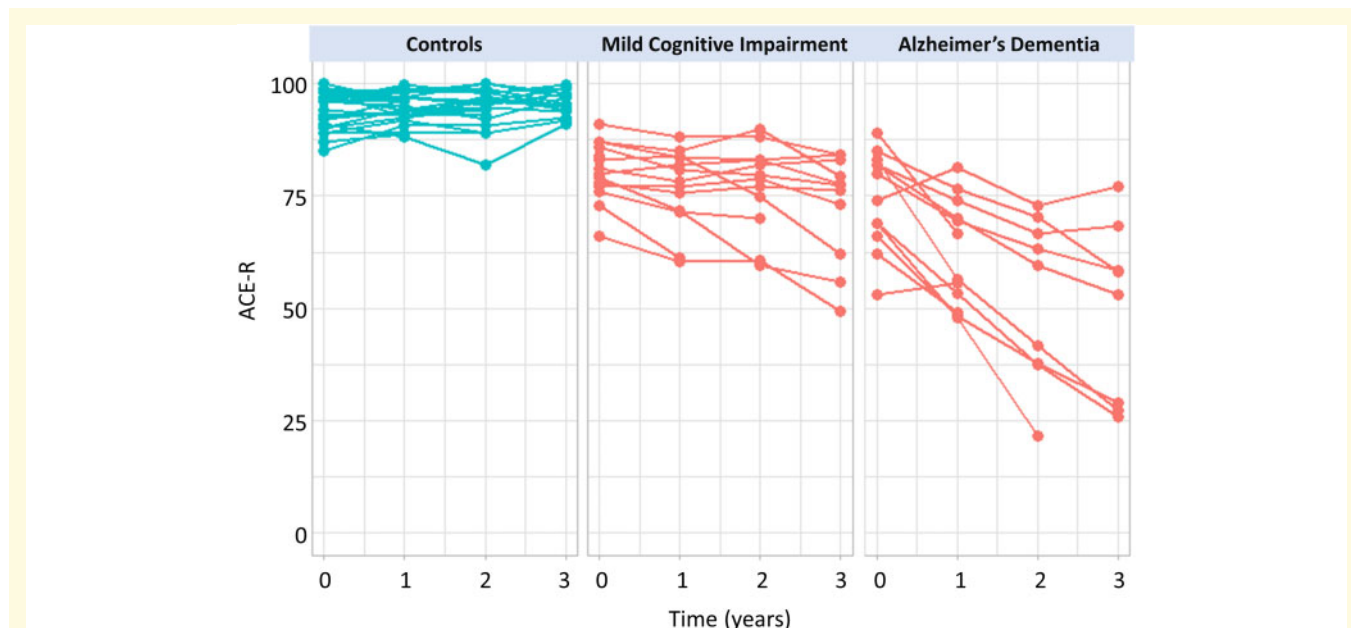


Figure 1 Longitudinal cognitive changes in patients and controls, as measured by the ACE-R. Points represent annualized ACE-R scores at baseline, and 1-year, 2-year and 3-year follow-ups for each subject in control (blue) and patient (red) groups.

One-step prediction LGCM with predictors

The LGCM including MRI fitted the data adequately [$\chi^2(10) = 18.33, P$ -value = 0.05, RMSEA = 0.13 (0.01–0.23), CFI = 0.98, SRMR = 0.03]. Inspecting the standardized residual matrices, none were greater than $r = 0.105$. Individual differences in the summary brain measure were strongly and positively associated with both slope (path Std Est = 0.58, $P < 0.001$) and intercept (path Std Est = 0.67, $P < 0.001$). This suggested that individuals with greater grey matter volumes showed better baseline performance, and slower longitudinal decline, than those with smaller volumes.

The LGCM of the posterior $^{18}\text{F-AV-1451}$ component fitted the data adequately [$\chi^2(10) = 16.30, P$ -value = 0.09, RMSEA = 0.12 (0.00–0.22), CFI = 0.98, SRMR = 0.03], and no single standardized residual was greater than $r = 0.101$. Here too, both the slope (path Std Est = $-0.62, P = 0.001$) and intercept (path Std Est = $-0.53, P < 0.001$)

were strongly governed by individual differences in the first component. In contrast, in the model with only the anterior $^{18}\text{F-AV-1451}$ component [$\chi^2(10) = 21.75, P$ -value = 0.01, RMSEA = 0.17 (0.07–0.27), CFI = 0.96, SRMR = 0.05], there was no association between the scores on the neural component and either the intercept (path Std Est = $-0.12, P = 0.431$) or the slope (path Std Est = $-0.39, P = 0.057$). In this model, no single standardized residual was greater than $r = 0.148$.

Finally, the LGCM with the anterior $^{11}\text{C-PK11195}$ component fitted the adequately [$\chi^2(10) = 16.32, P$ -value = 0.09, RMSEA = 0.13 (0.00–0.23), CFI = 0.97, SRMR = 0.02], and no single standardized residual was greater than $r = 0.056$. Individual differences in the $^{11}\text{C-PK11195}$ component governed both slope (Std Est = $-0.51, P = 0.002$) and intercept (Std Est = $-0.43, P < 0.001$) correlated with Component 1. In the model with the posterior $^{11}\text{C-PK11195}$ component as regressor, [$\chi^2(10) = 9.33, P$ -value = 0.50, RMSEA = 0.00 (0.00–0.17), CFI = 1.00, SRMR = 0.03], the slope resulted significantly correlated with the

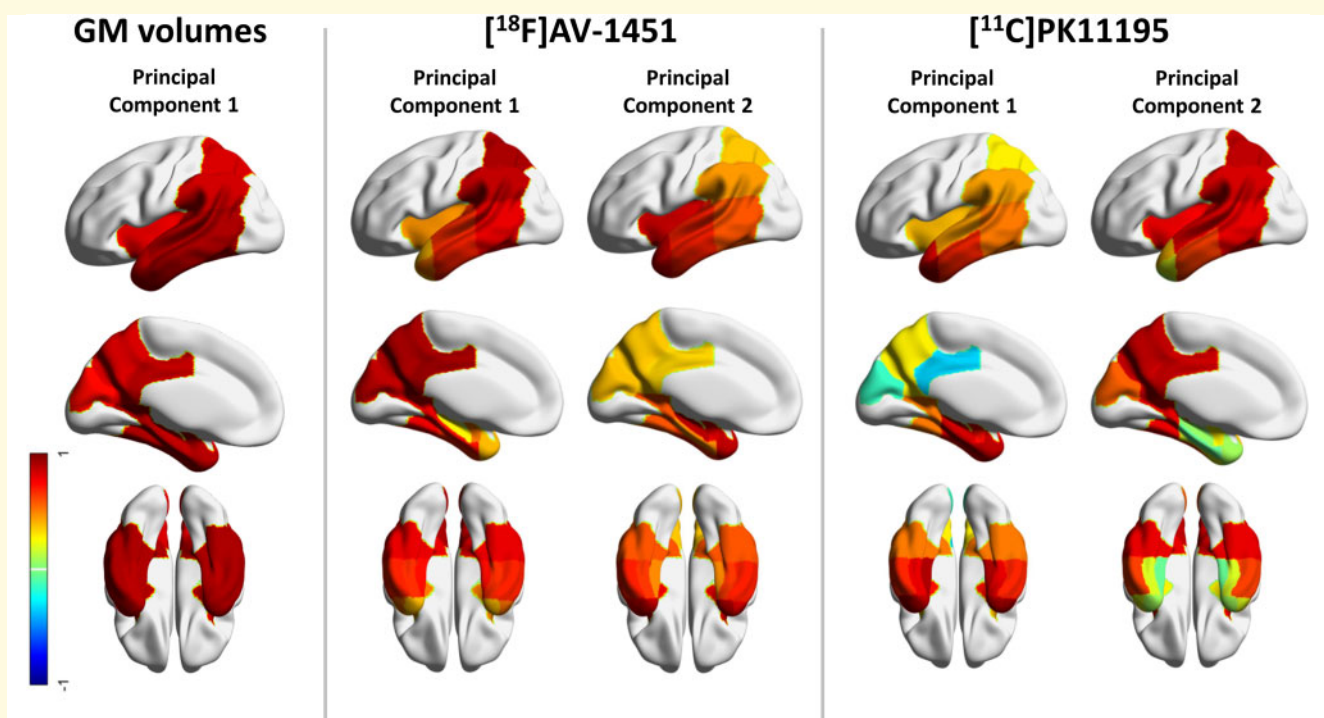


Figure 2 Principal components of the multimodal imaging. Regional weights of the structural MRI component (left), and rotated regional weights of ^{18}F -AV-1451 components (middle) and the ^{11}C -PK11195 components (right). Components were identified applying three independent principal component analyses on 15 temporo-parietal regions. For structural MRI, regional grey matter (GM) volumes were included in the analysis, while for each PET tracer, the binding potential values in those regions were considered, separately for each modality. The colours represent the region-specific weights (range: from -1 to 1) on each component (Supplementary Table 4).

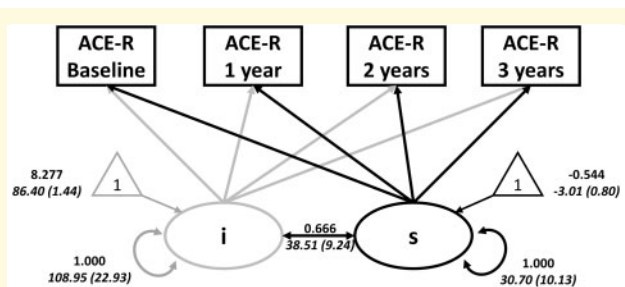


Figure 3 LGCM to test the initial values (intercept, 'i') and longitudinal changes (slope, 's') in scores of the ACE-R across all sample. Circles indicate latent variables, rectangles indicate observed variables, and triangles denote intercepts (1 = population means on the parameters). Thick single-headed arrows indicate regressions while thick double-headed arrows indicate variance and covariance (grey for intercept and black for slope). Values in Roman are standardized parameter estimates, and values in italics are unstandardized parameter estimates (with standard errors in parentheses). The annual rate of change was positively associated with performance at baseline (lower initial cognitive scores were associated with a higher annual rate of cognitive changes).

component (Std Est = -0.45 , $P = 0.009$), but not the intercept (Std Est = -0.010 , $P = 0.951$). No single standardized residual was greater than $r = 0.108$.

In patients, an LGCM including the components of all three imaging methods did not fit the data well [$\chi^2(18) = 34.76$, P -value = 0.01 , RMSEA = 0.17 (0.08 – 0.26), CFI = 0.92 , SRMR = 0.04], but no single standardized residual was greater than $r = 0.119$. With this caveat, cognitive decline (slope) was predicted by baseline posterior ^{18}F -AV-1451 (path Std Est = -0.49 , $P = 0.025$) and anterior ^{11}C -PK11195 (path Std Est = -0.40 , $P = 0.017$) components' scores, but not the posterior ^{11}C -PK11195, the MRI (path Std Est = 0.10 , $P = 0.52$) or the anterior ^{18}F -AV-1451 (Std Est = -0.22 , $P = 0.23$) components.

Two-step prediction: linear regression

Across all subjects, the rate of cognitive decline (slope from LGCM) was significantly associated with: (i) the MRI weighting (Std Beta = 0.61 , $P < 0.001$); (ii) the posterior ^{18}F -AV-1451 (Std Beta = -0.60 , $P < 0.001$); and (iii) anterior ^{11}C -PK11195 (Std Beta = -0.47 , $P = 0.002$). All these results survived Bonferroni's correction. Correlations of slope with the anterior ^{18}F -AV-1451 (Std Beta = -0.36 , $P = 0.022$), and the posterior ^{11}C -PK11195 (Std Beta = -0.39 , $P = 0.012$) did not survive correction for multiple comparisons ($P < 0.01$). Strikingly, these parameter estimates remained effectively unchanged even when

simultaneously including age, sex and education as covariates in the models (Supplementary Table 5). See Fig. 4 for a graphical representation of the significant associations between individual scores (x -axis) of imaging-specific principal components and slope in ACE-R scores (y -axis) extracted by LGCM. Model summary and coefficients for all univariable models with slope as dependent variable across the whole population are reported in Table 2. See Supplementary Table 6 for results from analysis of patients only.

In patients, the final model of multiple regression on cognitive slope (adjusted $R^2 = 0.418$, $SE = 4.18$; $P = 0.001$) included both ^{18}F -AV-1451 components (component 1: $Est = -2.57$, $SE = 0.71$, $P = 0.002$; component 2: $Est = -1.64$, $SE = 0.74$, $P = 0.038$), and the anterior ^{11}C -PK11195 (component 1: $Est = -1.92$, $SE = 0.74$, $P = 0.017$) as predictors (Fig. 5 and Table 3). Of note age, education, sex, the MRI component, and the posterior ^{11}C -PK11195 component were excluded from the final model.

Model summary and coefficients for both the initial model (adjusted $R^2 = 0.389$, $SE = 4.43$; $P = 0.027$), the full model with only brain predictors (adjusted $R^2 = 0.474$, $SE = 4.12$; $P = 0.002$), and the final model are reported in Supplementary Table 7. Either in the initial model with covariates or in the full model with only brain measures as predictors, the posterior ^{18}F -AV-1451 component and the anterior ^{11}C -PK11195 component showed the highest estimated coefficients (Supplementary Table 7). The interaction between the imaging components in the final model was not significant ($P > 0.05$ uncorrected). In addition, the reduced multiple regression analysis, with the first component of each imaging method only, included the ^{18}F -AV-1451 component ($Est = -2.42$, $SE = 0.77$, $P = 0.004$) and the ^{11}C -PK11195 component ($Est = -1.71$, $SE = 0.80$, $P = 0.042$) in the final model (adjusted $R^2 = 0.366$, $SE = 4.52$; $P = 0.002$), while the MRI component was discarded. Again, the interaction between the imaging components was not significant ($P > 0.05$ uncorrected).

Two-step Bayesian prediction

With all brain components and demographic variables as candidate predictors of cognitive decline, model comparison using Bayes factors indicated that the best model included both ^{18}F -AV-1451 components [component 1: mean (SD) = -2.15 (0.65); component 2: mean (SD) = -1.37 (0.68)], and the anterior ^{11}C -PK11195 component [mean (SD) = -1.61 (0.68)] as predictors ($BF_{10} = 46.56$; $R^2 = 0.52$). Hence, the best model in this statistical framework did not contain structural MRI data. See Table 3 for details on the final model and Supplementary Table 8 for a list of models evaluated and the corresponding BF_{10} . The reduced Bayesian regression analysis with only the first component of each imaging method as predictor was in accord with the frequentist approach. The best model identified with BF_{10} criteria was the one with only the posterior ^{18}F -AV-1451 and the anterior ^{11}C -PK11195 components only as predictors of slope ($BF_{10} = 20.81$; $R^2 = 0.42$), but not the MRI component.

Discussion

This study demonstrates the independent and combined value of neuroimaging biomarkers for tau pathology (^{18}F -AV-1451 PET), neuroinflammation (^{11}C -PK11195 PET) and brain atrophy (structural MRI), in predicting longitudinal cognitive decline in patients with Alzheimer's disease. Baseline markers for tau pathology, neuroinflammation and atrophy in temporo-parietal regions individually predicted cognitive decline, across the spectrum of severity MCI to Alzheimer's dementia. But, in a multivariable model, cognitive decline was only associated with higher baseline tau pathology in posterior temporo-parietal regions and increased neuroinflammation in the anterior temporal structures. Bayesian analysis confirmed the evidence against the

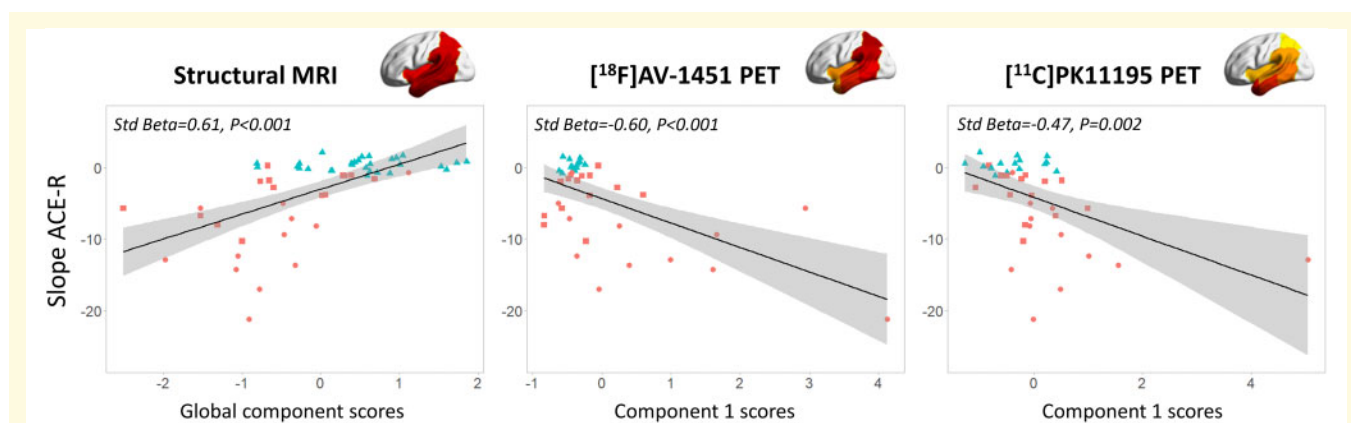


Figure 4 Imaging predictors of cognitive decline. Regression analyses with annual change in scores of the ACE-R (Slope ACE-R, y -axis) and individual baseline scores for each modality-specific principal component (x -axis): structural MRI (left), ^{18}F -AV-1451 PET (middle), and ^{11}C -PK11195 PET (right). Different colours represent different diagnostic groups: red circles = patients with Alzheimer's disease; red squares = patients with amyloid-positive MCI; controls = blue triangles.

Table 2 Results for the univariable regression models on slope across all populations

Model		Estimate	SE	Std Beta	t-value	P	Adjusted R ² (SE)	F	P
MRI (n = 55)	(Intercept)	-3.01	0.58		-5.23	0.000	0.358 (4.27)	31.18	<0.001*
	MRI component	3.48	0.63	0.61	5.58	0.000			
AV 1 (n = 40)	(Intercept)	-4.31	0.73	-	-5.88	0.000	0.341 (4.64)	21.22	<0.001*
	AV component 1	-3.43	0.74	-0.60	-4.61	0.000			
AV 2 (n = 40)	(Intercept)	-4.31	0.85	-	-5.05	0.000	0.108 (5.40)	5.72	0.022
	AV component 2	-2.08	0.87	-0.36	-2.39	0.022			
PK 1 (n = 41)	(Intercept)	-4.15	0.80	-	-5.19	0.000	0.204 (5.13)	11.26	0.002*
	PK component 1	-2.72	0.81	-0.47	-3.36	0.002			
PK 2 (n = 41)	(Intercept)	-4.15	0.84	-	-4.96	0.000	0.128 (5.36)	6.87	0.012
	PK component 2	-2.36	0.90	-0.39	-2.62	0.012			

AV = ¹⁸F-AV-1451; PK = ¹¹C-PK11195.

P = uncorrected P-values;

*Bonferroni corrected, significance threshold $P < 0.01$.

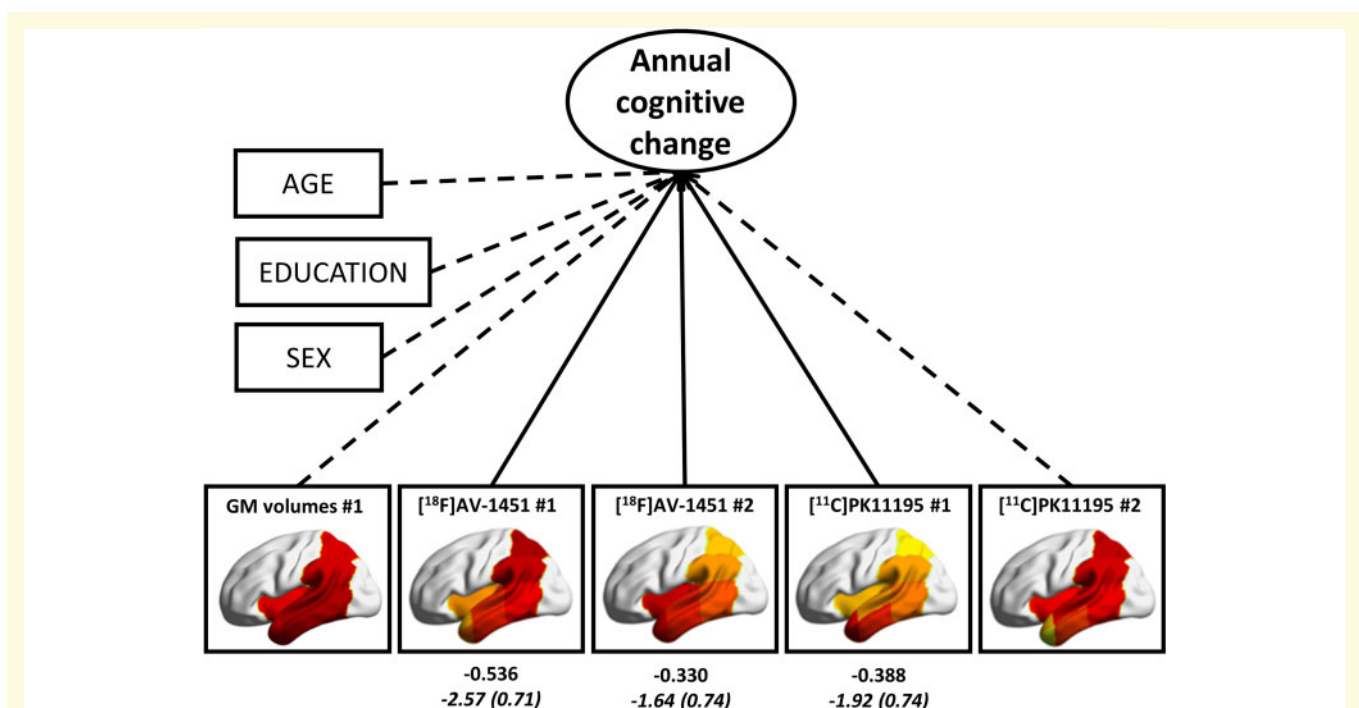


Figure 5 Results of the multiple linear regression in patients, with cognitive slope (annual cognitive change) extracted by the LGCM as dependent variable, and brain components' scores, age and education as independent variables. Solid arrows indicate significant coefficients of brain imaging measures indicated by the stepwise backward elimination, while dashed arrows indicate variables excluded by the final model. Values in Roman are standardized estimates, and values in italics are unstandardized beta estimates (standard errors in parentheses).

predictive value of MRI atrophy over and above the PET markers of tau pathology and neuroinflammation.

We used PCA to derive the most parsimonious neuroanatomical patterns of pathology that explain most of the imaging variance across the cohort. It is highly efficient for reducing data dimensionality and the problem of multiple comparisons. The PCA indicated two sets of regions (i.e. components) of co-varying tau pathology and neuroinflammation, in anterior versus posterior temporo-parietal regions. We focused on these regions because of their close

association with Alzheimer's disease (Garibotto et al., 2017; Jagust, 2018; Whitwell, 2018), but whole-brain regional data are available on request for other, exploratory, analyses. In patients, the degree of neuroinflammation and tau pathology did not correlate in either anterior or posterior temporo-parietal cortex. Previous studies have considered the *in vivo* association between these two pathological processes in prodromal and early Alzheimer's disease. Significant associations between tau and neuroinflammation measures have been reported in fronto-temporal regions (Dani et al.,

Table 3 Results of the multivariable regression models on the regression slope in patients

Frequentist regression								
Final model (Stepwise backward selection)	Estimate	SE	Std Beta	t-value	P	Adjusted R ² (SE)	F	P
(Intercept)	-5.41	0.87		-6.19	0.000	0.418 (4.18)	8.05	0.001
AV component 1	-2.57	0.71	-0.54	-3.60	0.002			
AV component 2	-1.64	0.74	-0.33	-2.21	0.038			
PK component 1	-1.92	0.74	-0.39	-2.59	0.017			
Bayesian regression								
Final model (BF-based selection)	Mean	SD	95% Credible interval		R ²	BF ₁₀		
			Lower	Upper				
(Intercept)	-6.82	0.82	-8.502	-5.129	0.523	46.56		
AV component 1	-2.15	0.65	-3.491	-0.802				
AV component 2	-1.37	0.68	-2.774	0.026				
PK component 1	-1.61	0.68	-3.001	-0.210				

For both frequentist (*top*) and Bayesian (*bottom*) the estimated coefficients for variables included in the final ('best') models are reported. AV = ¹⁸F-AV-1451; BF = Bayesian factor; PK = ¹¹C-PK11195.

2018), and parahippocampal cortex (Terada *et al.*, 2019). Using alternative ligands for tau and inflammation, ¹⁸F-MK-6240 and ¹¹C-PBR28, respectively, positive correlations were found in temporal, parietal and frontal cortex (Zou *et al.*, 2020). However, an earlier study failed to find significant correlations between tau and inflammation (Parbo *et al.*, 2018). Larger sample sizes may be needed to clarify the potential relationship, at different stages of disease.

The participants' weighting on atrophy, posterior ¹⁸F-AV-1451 and anterior ¹¹C-PK11195 components were separately associated with more rapid cognitive decline (Fig. 4 and Table 2). This result was confirmed by both the one- and two-step univariable prediction approaches. This corroborates the previously reported associations between cognitive deficits in Alzheimer's disease and the individual effects of tau pathology, neuroinflammation, and downstream cortical atrophy (Femminella *et al.*, 2016; Bejanin *et al.*, 2017; for reviews see Chandra *et al.*, 2019; Melis *et al.*, 2019). Although cross-sectional imaging studies with different PET ligands have reported single associations of cognitive performance with *in vivo* tau (Brier *et al.*, 2016; Cho *et al.*, 2016b; Johnson *et al.*, 2016; Ossenkoppele *et al.*, 2016; Pontecorvo *et al.*, 2017; Zou *et al.*, 2020; for a review see Chandra *et al.*, 2019) and microglial activation (Edison *et al.*, 2008; Okello *et al.*, 2009a; Fan *et al.*, 2015a; Passamonti *et al.*, 2018, 2019; Zou *et al.*, 2020; for a review see Chandra *et al.*, 2019), less is known about their relationship to longitudinal cognitive decline. Previous PET studies in Alzheimer's dementia and MCI reported that baseline ¹⁸F-AV-1451 PET uptake correlates with cognitive decline over a period of 6 (Koychev *et al.*, 2017) or 18 months (Pontecorvo *et al.*, 2019). Conversely, microglial activation showed progression over 14–16 months (Fan *et al.*, 2015b, 2017), although the predictive value of baseline measures was not reported. Other studies using ¹¹C-PBR28 to quantify neuroinflammation over a period of at least 1 year

(median 2.7 years) in MCI and Alzheimer's disease reported increased microglial activation as a function of a significant worsening on the Clinical Dementia Rating scale (Kreisl *et al.*, 2016). Likewise, binding of ¹⁸F-DPA-714, another TSPO PET ligand, is negatively associated with cognitive performance (Hamelin *et al.*, 2018).

Improving our knowledge of how baseline measures of tau, neuroinflammation, and brain atrophy predict cognitive decline in Alzheimer's disease may inform future cost-effectiveness of studies in large and epidemiologically representative cohorts of patients. Although other studies have assessed the predictive value of different brain markers on longitudinal cognitive decline in Alzheimer's disease (for reviews see Chandra *et al.*, 2019; Melis *et al.*, 2019), this study compared the three biomarkers simultaneously (i.e. tau pathology, neuroinflammation, brain atrophy) in patients with amyloid-positive MCI and Alzheimer's dementia. Our data indicate the added value of PET imaging over and above MRI prognostic markers. Although brain atrophy in isolation is predictive for cognitive decline in Alzheimer's disease (Jack *et al.*, 2015), when models include tau burden, microglial activation and atrophy jointly, only PET was predictive (Fig. 5 and Table 3). This critical result was confirmed by both frequentist and Bayesian analyses, with evidence against the added value of MRI data on predicting cognitive decline over and above PET assessments. This aligns with cross-sectional studies that report a stronger association of tau molecular imaging than structural MRI with cognitive performance in patients with Alzheimer's disease (Bejanin *et al.*, 2017; Mattsson *et al.*, 2019). More specifically, in patients with MCI and Alzheimer's dementia, Benjanin and colleagues (2017) reported an association between regional tau PET binding and cognitive impairment, which was partly mediated by grey matter volumes. Cognition was equally explained by brain atrophy and tau pathology, but after accounting for grey matter values, *in vivo* tau

pathology remained correlated with cognitive performance (Bejanin *et al.*, 2017). Likewise, Mattsson *et al.* (2019) found that both ^{18}F -AV-1451 PET and structural brain MRI are associated with cognition in Alzheimer's disease (spanning preclinical, prodromal, and dementia stages), although associations of tau PET indices were stronger than those for MRI markers (Mattsson *et al.*, 2019).

Our data suggest that posterior temporo-parietal ^{18}F -AV-1451 binding and anterior temporal ^{11}C -PK11195 binding are associated with cognitive decline. In our cohort, they do not interact in their association with cognitive decline, which suggests an additive and independent effect of the two pathological processes on clinical progression, rather than synergy. In patients with Alzheimer's disease, temporo-parietal cortical tau PET signal is consistent with Braak stage III and above, while in cognitively healthy older individuals, the signal is localized to entorhinal cortex and inferior temporal cortex (Cho *et al.*, 2016a; Johnson *et al.*, 2016; for a review see Jagust, 2018). Post-mortem studies have likewise reported tau deposition in the medial temporal cortex in healthy elderly individuals and patients with Alzheimer's dementia (Jagust, 2018). Tau burden in the entorhinal, limbic, and temporal neocortex relates to cortical atrophy in patients with MCI and Alzheimer's disease, although not in cognitively normal controls (Timmers *et al.*, 2019). These findings suggest that tauopathy in the medial part of the temporal lobe may be an age-related norm, rather than indicative of Alzheimer's disease cognitive decline (Femminella *et al.*, 2018). For this reason, tau PET binding here may be a weaker predictor for cognitive decline than tau in the posterior temporo-parietal regions. The co-occurrence with amyloid- β and neuroinflammation may induce the tau spreading from the medial temporal lobe to other cortical regions, which may be associated with downstream neurodegenerative processes and cognitive decline (Mhatre *et al.*, 2015; Jagust, 2018; Perea *et al.*, 2018). This suggests a driving role of neuroinflammation in tau spread and neurodegeneration in Alzheimer's disease (Yoshiyama *et al.*, 2007; Asai *et al.*, 2015; Maphis *et al.*, 2015), in which activated microglia facilitate tau spread (Maphis *et al.*, 2015; Perea *et al.*, 2018). In addition, it is possible that the relationships between tau, neuroinflammation and cognitive progression are not constant, and that the PET biomarkers would have different prognostic relevance during pre-symptomatic, prodromal and dementia stages of Alzheimer's disease. Larger studies, or meta-analyses, would be required for adequate power to test such dynamic prognostic models.

There are limitations to our study. TSPO expression in neuroinflammation cascade is complex, and has been found not only in activated microglia but also in other cell types, such as astrocytes and vascular smooth muscle cells (Gui *et al.*, 2019). However, ^{11}C -PK11195 is selective for activated microglia over quiescent microglia and reactive astrocytes (Banati, 2002), which favours its utility for imaging activated microglia. In this context, several second-generation PET radioligands for TSPO have been developed since ^{11}C -PK11195 (e.g. ^{11}C -PBR28 and ^{18}F -DPA-714), and used

in human studies (Vivash and O'Brien, 2016). They are characterized by higher signal-to-noise ratio and lower lipophilicity than ^{11}C -PK11195. However, they require genetic analysis to assess a single-nucleotide polymorphism (rs6971), which influences their binding affinity and causes heterogeneity in PET data (Dupont *et al.*, 2017). ^{11}C -PK11195 is less affected by this genetic polymorphism, especially between high and mixed affinity binders (Guo *et al.*, 2012; Kobayashi *et al.*, 2018) that represent $\sim 90\%$ of the Caucasian population (Owen *et al.*, 2012), although a small difference in ^{11}C -PK11195 binding in the CNS remains a possibility (Fujita *et al.*, 2017). Second, the cross-sectional nature of our imaging assessment does not enable a mediation analysis, or support inferences on the direction of causality between tau pathology, microglial activation progression and cognitive decline. However, both processes predict the rate of cognitive deterioration in Alzheimer's disease. Third, the modest sample size of our cohort limited the applicability of the one-step prediction procedure with multiple predictors, which may lead to a more precise prediction than the two-step procedures. For the multivariable regression model the sample size was reduced to $n = 26$ because of the exclusion of controls (who underwent ^{18}F -AV-1451 or ^{11}C -PK11195 PET, but not both, to limit radiation exposure). However, both frequentist and Bayesian multivariable approaches give similar results, aligning with those obtained by the one-step prediction. The convergence between the statistical models (i.e. LGCM with predictors, linear regression and Bayesian model) mitigates against sample-dependent biases on the estimation of the most parsimonious model. The replication of these findings with larger and multicentre clinical cohorts will represent an important next step to establish the replicability and generalizability of our results. Fourth, the interval between cognitive assessment and imaging varied. However, we sought to mitigate this confound by including the interval in the statistical analyses, and note that the intervals were small compared with the 3-year follow up.

We conclude that PET markers of regional pathological processes are stronger predictors than atrophy, as measured by MRI, of clinical progression in patients with symptomatic Alzheimer's disease. The predictive models were convergent in identifying tau burden in posterior cortical regions and neuroinflammation in the anterior temporal lobe as imaging predictors of cognitive decline in the clinical spectrum of Alzheimer's disease. In contrast, atrophy predicted cognitive decline only if considered individually but not over and above the effects of tau burden and inflammation. Our findings support the use of PET imaging of tau pathology and microglial activation for prognostication and patients' stratification in clinical trials.

Acknowledgements

We thank our participant volunteers for their participation in this study, and the radiographers/technologists at the

Wolfson Brain Imaging Centre and Addenbrooke's PET/CT Unit, and the research nurses of the Cambridge Centre for Frontotemporal Dementia and Related Disorders for their invaluable support in data acquisition. We thank the East Anglia Dementias and Neurodegenerative Diseases Research Network (DeNDROn) for help with subject recruitment, and Drs Istvan Boros, Joong-Hyun Chun, and other WBIC RPU staff for the manufacture of the radioligands. We thank Avid (Lilly) for supplying the precursor for the production of ^{18}F -AV-1451 used in this study.

Funding

This study was co-funded by the NIHR Cambridge Biomedical Research Centre Dementia and Neurodegeneration theme; the Wellcome Trust (103838); the Cambridge Trust & Sidney Sussex College Scholarship; the Medical Research Council (SUAG/04/G101400; and MR/P01271X/1); the Cambridge Centre for Parkinson Plus, and British Academy (PF160048). The views expressed are those of the authors and not necessarily those of the NIHR or the Department of Health and Social Care.

Competing interests

J.B.R. reports consultancy unrelated to the work with Biogen, UCB, Asceneuron and Althira; and receipt of research grants from Janssen, AZ-Medimmune, Lilly unrelated to this work. J.O.B. has provided consultancy to TauRx, Axon, Roche, GE Healthcare, Lilly and has research awards from Alliance Medical and Merck.

Supplementary material

Supplementary material is available at *Brain* online.

References

Albert MS, DeKosky ST, Dickson D, Dubois B, Feldman HH, Fox NC, et al. The diagnosis of mild cognitive impairment due to Alzheimer's disease: recommendations from the National Institute on Aging-Alzheimer's Association workgroups on. *Alzheimer's Dement* 2011; 7: 270–9.

Asai H, Ikezu S, Tsunoda S, Medalla M, Luebke J, Haydar T, et al. Depletion of microglia and inhibition of exosome synthesis halt tau propagation. *Nat Neurosci* 2015; 18: 1584–93.

Aschenbrenner AJ, Gordon BA, Benzinger TLS, Morris JC, Hassenstab JJ. Influence of tau PET, amyloid PET, and hippocampal volume on cognition in Alzheimer disease. *Neurology* 2018; 91: e859–66.

Banati RB. Visualising microglial activation in vivo. *Glia* 2002; 40: 206–17.

Bejanin A, Schonhaut DR, La Joie R, Kramer JH, Baker SL, Sosa N, et al. Tau pathology and neurodegeneration contribute to cognitive impairment in Alzheimer's disease. *Brain* 2017; 140: 3286–300.

Bentler PM, Chou CP. Practical issues in structural modeling. *Sociol Methods Res* 1987; 16: 78–117.

Bevan-Jones WR, Surendranathan A, Passamonti L, Vázquez Rodríguez P, Arnold R, Mak E, et al. Neuroimaging of Inflammation in Memory and Related Other Disorders (NIMROD) study protocol: a deep phenotyping cohort study of the role of brain inflammation in dementia, depression and other neurological illnesses. *BMJ Open* 2017; 7: e013187.

Brier MR, Gordon B, Friedrichsen K, McCarthy J, Stern A, Christensen J, et al. Tau and A β imaging, CSF measures, and cognition in Alzheimer's disease. *Sci Transl Med* 2016; 8: 338ra66.

Calsolaro V, Edison P. Neuroinflammation in Alzheimer's disease: current evidence and future directions. *Alzheimer's Dement* 2016; 12: 719–32.

Chandra A, Gennaro PV, Oliver P. Applications of amyloid, tau, and neuroinflammation PET imaging to Alzheimer's disease and mild cognitive impairment. *Hum Brain Mapp* 2019; 40: 1–19.

Chiotis K, Saint-Aubert L, Rodriguez-Vieitez E, Leuz A, Almkvist O, Savitcheva I, et al. Longitudinal changes of tau PET imaging in relation to hypometabolism in prodromal and Alzheimer's disease dementia. *Mol Psychiatry* 2018; 23: 1666–73.

Cho H, Choi JY, Hwang MS, Kim YJ, Lee HM, Lee HS, et al. In vivo cortical spreading pattern of tau and amyloid in the Alzheimer disease spectrum. *Ann Neurol* 2016; 80: 247–58.

Cho H, Choi JY, Hwang M, Lee JH, Kim YJ, Lee HM, et al. Tau PET in Alzheimer disease and mild cognitive impairment. *Neurology* 2016; 87: 375–83.

Cho H, Choi JY, Lee HS, Lee J-H, Ryu YH, Lee MS, et al. Progressive tau accumulation in Alzheimer's disease: two-year follow-up study. *J Nucl Med* 2019; 60: 1611–21.

Dani M, Wood M, Mizoguchi R, Fan Z, Walker Z, Morgan R, et al. Microglial activation correlates in vivo with both tau and amyloid in Alzheimer's disease. *Brain* 2018; 141: 2740–54.

Dupont A-C, Largeau B, Santiago Ribeiro M, Guilloteau D, Tronel C, Arlicot N. Translocator protein-18 kDa (TSPO) positron emission tomography (PET) imaging and its clinical impact in neurodegenerative diseases. *Int J Mol Sci* 2017; 18: 785.

Edison P, Archer H. A, Gerhard A, Hinz R, Pavese N, Turkheimer FE, et al. Microglia, amyloid, and cognition in Alzheimer's disease: an [^{11}C](R)PK11195-PET and [^{11}C]PIB-PET study. *Neurobiol Dis* 2008; 32: 412–9.

Fan Z, Aman Y, Ahmed I, Chetelat G, Landeau B, Ray Chaudhuri K, et al. Influence of microglial activation on neuronal function in Alzheimer's and Parkinson's disease dementia. *Alzheimer's Dement* 2015; 11: 608–21.e7.

Fan Z, Brooks DJ, Okello A, Edison P. An early and late peak in microglial activation in Alzheimer's disease trajectory. *Brain* 2017; 140: 792–803.

Fan Z, Okello AA, Brooks DJ, Edison P. Longitudinal influence of microglial activation and amyloid on neuronal function in Alzheimer's disease. *Brain* 2015; 138: 3685–98.

Femminella GD, Ninan S, Atkinson R, Fan Z, Brooks DJ, Edison P. Does microglial activation influence hippocampal volume and neuronal function in Alzheimer's disease and Parkinson's disease dementia? *J Alzheimer's Dis* 2016; 51: 1275–89.

Femminella GD, Thayanandan T, Calsolaro V, Komici K, Rengo G, Corbi G, et al. Imaging and molecular mechanisms of Alzheimer's disease: a review. *Int J Mol Sci* 2018; 19. doi: 10.3390/ijms19123702.

Frisoni GB, Fox NC, Jack CR, Scheltens P, Thompson PM. The clinical use of structural MRI in Alzheimer disease. *Nat Rev Neurol* 2010; 6: 67–77.

Fujita M, Kobayashi M, Ikawa M, Gunn RN, Rabiner EA, Owen DR, et al. Comparison of four ^{11}C -labeled PET ligands to quantify translocator protein 18 kDa (TSPO) in human brain: (R)-PK11195, PBR28, DPA-713, and ER176—based on recent publications that measured specific-to-non-displaceable ratios. *EJNMMI Res* 2017; 7: 84.

Garibotto V, Herholz K, Boccardi M, Picco A, Varrone A, Nordberg A, et al. Clinical validity of brain fluorodeoxyglucose positron

- emission tomography as a biomarker for Alzheimer's disease in the context of a structured 5-phase development framework. *Neurobiol Aging* 2017; 52: 183–95.
- Gousias IS, Rueckert D, Heckemann RA, Dyet LE, Boardman JP, Edwards AD, et al. Automatic segmentation of brain MRIs of 2-year-olds into 83 regions of interest. *Neuroimage* 2008; 40: 672–84.
- Gui Y, Marks JD, Das S, Hyman BT, Serrano-Pozo A. Characterization of the 18 kDa translocator protein (TSPO) expression in post-mortem normal and Alzheimer's disease brains. *Brain Pathol* 2019; 30: 151–64.
- Gunn RN, Lammertsma AA, Hume SP, Cunningham VJ. Parametric imaging of ligand-receptor binding in PET using a simplified reference region model. *Neuroimage* 1997; 6: 279–87.
- Guo Q, Owen DR, Rabiner EA, Turkheimer FE, Gunn RN. Identifying improved TSPO PET imaging probes through biomathematics: the impact of multiple TSPO binding sites in vivo. *Neuroimage* 2012; 60: 902–10.
- Hall B, Mak E, Cervenka S, Aigbirhio FI, Rowe JB, O'Brien JT. In vivo tau PET imaging in dementia: pathophysiology, radiotracer quantification, and a systematic review of clinical findings. *Ageing Res Rev* 2017; 36: 50–63.
- Hamelin L, Lagarde J, Dorothée G, Potier MC, Corlier F, Kuhnast B, et al. Distinct dynamic profiles of microglial activation are associated with progression of Alzheimer's disease. *Brain* 2018; 141: 1855–70.
- Hammers A, Allom R, Koeppe MJ, Free SL, Myers R, Lemieux L, et al. Three-dimensional maximum probability atlas of the human brain, with particular reference to the temporal lobe. *Hum Brain Mapp* 2003; 19: 224–47.
- Heneka MT, Carson MJ, Khoury J, El Landreth GE, Brosseron F, Feinstein DL, et al. Neuroinflammation in Alzheimer's disease. *Lancet Neurol* 2015; 14: 388–405.
- Jack CR, Barnes J, Bernstein MA, Borowski BJ, Brewer J, Clegg S, et al. Magnetic resonance imaging in Alzheimer's Disease neuroimaging initiative 2. *Alzheimer's Dement* 2015; 11: 740–56.
- Jack CR, Lowe VJ, Senjem ML, Weigand SD, Kemp BJ, Shiung MM, et al. 11C PiB and structural MRI provide complementary information in imaging of Alzheimer's disease and amnesic mild cognitive impairment. *Brain* 2008; 131: 665–80.
- Jack CR, Wiste HJ, Schwarz CG, Lowe VJ, Senjem ML, Vemuri P, et al. Longitudinal tau PET in ageing and Alzheimer's disease. *Brain* 2018; 141: 1517–28.
- Jagust W. Imaging the evolution and pathophysiology of Alzheimer disease. *Nat Rev Neurosci* 2018; 19: 687–700.
- Johnson K. A, Schultz A, Betensky R. A, Becker JA, Sepulcre J, Rentz D, et al. Tau positron emission tomographic imaging in aging and early Alzheimer disease. *Ann Neurol* 2016; 79: 110–19.
- Kinahan PE, Rogers JG. Analytic 3D image reconstruction using all detected events. *IEEE Trans Nucl Sci* 1989; 36: 964–8.
- Klunk WE, Engler H, Nordberg A, Wang Y, Blomqvist G, Holt DP, et al. Imaging brain amyloid in Alzheimer's disease with Pittsburgh Compound-B. *Ann Neurol* 2004; 55: 306–19.
- Kobayashi M, Jiang T, Telu S, Zoghbi SS, Gunn RN, Rabiner EA, et al. 11 C-DPA-713 has much greater specific binding to translocator protein 18 kDa (TSPO) in human brain than 11 C- (R) - PK11195. *J Cereb Blood Flow Metab* 2018; 38: 393–403.
- Koychev I, Gunn RN, Firouzian A, Lawson J, Zamboni G, Ridha B, et al. PET Tau and Amyloid- β Burden in Mild Alzheimer's Disease: divergent relationship with age, cognition, and cerebrospinal fluid biomarkers. *J Alzheimer's Dis* 2017; 60: 283–93.
- Kreisl WC, Lyoo CH, Liow J-S, Wei M, Snow J, Page E, et al. 11C-PBR28 binding to translocator protein increases with progression of Alzheimer's disease. *Neurobiol Aging* 2016; 44: 53–61.
- Leung KK, Bartlett JW, Barnes J, Manning EN, Ourselin S, Fox NC. Cerebral atrophy in mild cognitive impairment and Alzheimer disease: rates and acceleration. *Neurology* 2013; 80: 648–54.
- Lowe VJ, Curran G, Fang P, Liesinger AM, Josephs K. A, Parisi JE, et al. An autoradiographic evaluation of AV-1451 Tau PET in dementia. *Acta Neuropathol Commun* 2016; 4: 19.
- Lowe VJ, Lundt ES, Albertson SM, Min H-K, Fang P, Przybelski SA, et al. Tau-positron emission tomography correlates with neuropathology findings [Internet]. *Alzheimer's Dement* 2020; 16: 561–71.
- Maass A, Lockhart SN, Harrison TM, Bell RK, Mellinger T, Swinnerton K, et al. Entorhinal tau pathology, episodic memory decline, and neurodegeneration in aging. *J Neurosci* 2018; 38: 530–43.
- Maphis N, Xu G, Kokiko-Cochran ON, Jiang S, Cardona A, Ransohoff RM, et al. Reactive microglia drive tau pathology and contribute to the spreading of pathological tau in the brain. *Brain* 2015; 138: 1738–55.
- Marquié M, Normandin MD, Vanderburg CR, Costantino IM, Bien EA, Rycyna LG, et al. Validating novel tau positron emission tomography tracer [F-18]-AV-1451 (T807) on postmortem brain tissue. *Ann Neurol* 2015; 78: 787–800.
- Mattsson N, Insel PS, Donohue M, Jögi J, Ossenkoppele R, Olsson T, et al. Predicting diagnosis and cognition with 18 F-AV-1451 tau PET and structural MRI in Alzheimer's disease. *Alzheimer's Dement* 2019; 15: 570–80.
- McKhann GM, Knopman DS, Chertkow H, Hyman BT, Jack CR, Kawas CH, et al. The diagnosis of dementia due to Alzheimer's disease: recommendations from the National Institute on Aging-Alzheimer's Association workgroups on diagnostic guidelines for Alzheimer's disease. *Alzheimer's Dement* 2011; 7: 263–9.
- Melis RJJ, Haakma ML, Muniz-Terrera G. Understanding and predicting the longitudinal course of dementia. *Curr Opin Psychiatry* 2019; 32: 123–9.
- Mhatre SD, Tsai CA, Rubin AJ, James ML, Andreasson KI. Microglial Malfunction: the Third Rail in the Development of Alzheimer's Disease. *Trends Neurosci* 2015; 38: 621–36.
- Mioshi E, Dawson K, Mitchell J, Arnold R, Hodges JR. The Addenbrooke's Cognitive Examination Revised (ACE-R): a brief cognitive test battery for dementia screening. *Int J Geriatr Psychiatry* 2006; 21: 1078–85.
- Nelson PT, Alafuzoff I, Bigio EH, Bouras C, Braak H, Cairns NJ, et al. Correlation of Alzheimer Disease Neuropathologic Changes With Cognitive Status: a Review of the Literature. *J Neuropathol Exp Neurol* 2012; 71: 362–81.
- Newsom JT. Longitudinal structural equation modeling: a comprehensive introduction. New York: Routledge; 2015.
- Okello A, Edison P, Archer H. A, Turkheimer FE, Kennedy J, Bullock R, et al. Microglial activation and amyloid deposition in mild cognitive impairment: a PET study. *Neurology* 2009; 72: 56–62.
- Okello A, Koivunen J, Edison P, Archer HA, Turkheimer FE, Nägren K, et al. Conversion of amyloid positive and negative mci to ad over 3 years: an c-pib pet study symbol. *Neurology* 2009; 73: 754–60.
- Ossenkoppele R, Schonhaut DR, Schöll M, Lockhart SN, Ayakta N, Baker SL, et al. Tau PET patterns mirror clinical and neuroanatomical variability in Alzheimer's disease. *Brain* 2016; 139: 1551–67.
- Owen DR, Yeo AJ, Gunn RN, Song K, Wadsworth G, Lewis A, et al. An 18-kDa translocator protein (TSPO) polymorphism explains differences in binding affinity of the PET radioligand PBR28. *J Cereb Blood Flow Metab* 2012; 32: 1–5.
- Parbo P, Ismail R, Sommerauer M, Stokholm MG, Hansen AK, Hansen KV, et al. Does inflammation precede tau aggregation in early Alzheimer's disease? A PET study. *Neurobiol Dis* 2018; 117: 211–6.
- Pasqualetti G, Brooks DJ, Edison P. The Role of Neuroinflammation in Dementias. *Curr Neurol Neurosci Rep* 2015; 15: 17.
- Passamonti L, Rodríguez PV, Hong YT, Allinson KSJ, Bevan-Jones WR, Williamson D, et al. 11 CPK11195 binding in Alzheimer disease and progressive supranuclear palsy. *Neurology* 2018; 90: e1989–96.
- Passamonti L, Tsvetanov KA, Jones PS, Bevan-Jones WR, Arnold R, Borchert RJ, et al. Neuroinflammation and functional connectivity in Alzheimer's Disease: interactive influences on cognitive performance. *J Neurosci* 2019; 39: 7218–26.
- Passamonti L, Vázquez Rodríguez P, Hong YT, Allinson KSJ, Williamson D, Borchert RJ, et al. ¹⁸ F-AV-1451 positron emission

- tomography in Alzheimer's disease and progressive supranuclear palsy. *Brain* 2017; 140: 781–91.
- Perea JR, Llorens-Martín M, Ávila J, Bolós M. The Role of Microglia in the Spread of Trelevance for Tauopathies. *Front Cell Neurosci* 2018; 12: 1–8.
- Pontecorvo MJ, Devous MD, Kennedy I, Navitsky M, Lu M, Galante N, et al. A multicentre longitudinal study of flortaucipir (18F) in normal ageing, mild cognitive impairment and Alzheimer's disease dementia. *Brain* 2019; 142: 1723–35.
- Pontecorvo MJ, Devous MD, Navitsky M, Lu M, Salloway S, Schaerf FW, et al. Relationships between flortaucipir PET tau binding and amyloid burden, clinical diagnosis, age and cognition. *Brain* 2017; 140: 748–63.
- Ransohoff RM. How neuroinflammation contributes to neurodegeneration. *Science* (80-) 2016; 353: 777–83.
- Raz N, Lindenberger U, Rodrigue KM, Kennedy KM, Head D, Williamson A, et al. Regional brain changes in aging healthy adults: general trends, individual differences and modifiers. *Cereb Cortex* 2005; 15: 1676–89.
- Rosseel Y. lavaan: an R Package for Structural Equation Modeling. *J Stat Softw* 2012; 48: 1–36.
- Sander K, Lashley T, Gami P, Gendron T, Lythgoe MF, Rohrer JD, et al. Characterization of tau positron emission tomography tracer [18F]AV-1451 binding to postmortem tissue in Alzheimer's disease, primary tauopathies, and other dementias. *Alzheimer's Dement* 2016; 12: 1116–24.
- Scarf AM, Kassiou M. The translocator protein. *J Nucl Med* 2011; 52: 677–80.
- Schain M, Kreisl WC. Neuroinflammation in neurodegenerative disorders—a review. *Curr Neurol Neurosci Rep* 2017; 17: 25.
- Schermelleh-Engel K, Moosbrugger H, Müller H. Evaluating the fit of structural equation models: tests of significance and descriptive goodness-of-fit measures. *Methods Psychol Res* 2003; 8: 23–74.
- Schöll M, Lockhart SN, Schonhaut DR, O'Neil JP, Janabi M, Ossenkuppele R, et al. PET imaging of tau deposition in the aging human brain. *Neuron* 2016; 89: 971–82.
- Schöll M, Maass A, Mattsson N, Ashton NJ, Blennow K, Zetterberg H, et al. Biomarkers for tau pathology. *Mol Cell Neurosci* 2019; 97: 18–33.
- Schwarz AJ, Yu P, Miller BB, Shcherbinin S, Dickson J, Navitsky M, et al. Regional profiles of the candidate tau PET ligand 18F-AV-1451 recapitulate key features of Braak histopathological stages. *Brain* 2016; 139: 1539–50.
- Smith R, Wibom M, Pawlik D, Englund E, Hansson O. Correlation of in Vivo [18 F]Flortaucipir with postmortem Alzheimer disease tau pathology. *JAMA Neurol* 2019; 76: 310–17.
- Southekal S, Devous MD, Kennedy I, Navitsky M, Lu M, Joshi AD, et al. Flortaucipir F 18 quantitation using parametric estimation of reference signal intensity. *J Nucl Med* 2018; 59: 944–51.
- Spires-Jones TL, Hyman BT. The intersection of amyloid beta and tau at synapses in Alzheimer's disease. *Neuron* 2014; 82: 756–71.
- Stefaniak J, O'Brien J. Imaging of neuroinflammation in dementia: a review. *J Neurol Neurosurg Psychiatry* 2015; 87: 21–8.
- Terada T, Yokokura M, Obi T, Bunai T, Yoshikawa E, Ando I, et al. In vivo direct relation of tau pathology with neuroinflammation in early Alzheimer's disease [Internet]. *J Neurol* 2019; 266: 2186–96.
- Timmers T, Ossenkuppele R, Wolters EE, Verfaillie SCJ, Visser D, Golla SSV, et al. Associations between quantitative [18F]flortaucipir tau PET and atrophy across the Alzheimer's disease spectrum. *Alzheimers Res Ther* 2019; 11: 60.
- Villemagne VL, Burnham S, Bourgeat P, Brown B, Ellis KA, Salvado O, et al. Amyloid β deposition, neurodegeneration, and cognitive decline in sporadic Alzheimer's disease: A prospective cohort study. *Lancet Neurol* 2013; 12: 357–67.
- Villemagne VL, Pike KE, Chételat G, Ellis KA, Mulligan RS, Bourgeat P, et al. Longitudinal assessment of A β and cognition in aging and Alzheimer disease. *Ann Neurol* 2011; 69: 181–92.
- Vivash L, O'Brien TJ. Imaging Microglial Activation with TSPO PET: lighting up neurologic diseases? *J Nucl Med* 2016; 57: 165–8.
- Walhovd KB, Westlye LT, Amlien I, Espeseth T, Reinvang I, Raz N, et al. Consistent neuroanatomical age-related volume differences across multiple samples. *Neurobiol Aging* 2011; 32: 916–32.
- Whitwell JL. Alzheimer 's disease neuroimaging. *Curr Opin Neurol* 2018; 31: 396–404.
- Xia CF, Arteaga J, Chen G, Gangadharmath U, Gomez LF, Kasi D, et al. 18F]T807, a novel tau positron emission tomography imaging agent for Alzheimer's disease. *Alzheimer's Dement* 2013; 9: 666–76.
- Yaqub M, Van Berckel BNM, Schuitemaker A, Hinz R, Turkheimer FE, Tomasi G, et al. Optimization of supervised cluster analysis for extracting reference tissue input curves in (R)-[11C]PK11195 brain PET studies. *J Cereb Blood Flow Metab* 2012; 32: 1600–8.
- Yokokura M, Mori N, Yagi S, Yoshikawa E, Kikuchi M, Yoshihara Y, et al. In vivo changes in microglial activation and amyloid deposits in brain regions with hypometabolism in Alzheimer's disease. *Eur J Nucl Med Mol Imaging* 2011; 38: 343–51.
- Yoshiyama Y, Higuchi M, Zhang B, Huang SM, Iwata N, Saido TCC, et al. Synapse Loss and Microglial Activation Precede Tangles in a P301S Tauopathy Mouse Model. *Neuron* 2007; 53: 337–51.
- Zou J, Tao S, Johnson A, Tomljanovic Z, Polly K, Klein J, et al. Microglial activation, but not tau pathology, is independently associated with amyloid positivity and memory impairment. *Neurobiol Aging* 2020; 85: 11–21.